Available online at www.sciencedirect.com

ScienceDirect

Energy Procedia 92 (2016) 493 – 499

Energy Procedia

6th International Conference on Silicon Photovoltaics, SiliconPV 2016

Flexible modules using <70 μm thick silicon solar cells

André Augusto, Kevin Tyler, Stanislau Y. Herasimenka, and Stuart G. Bowden

School of Electrical, Computer and Energy Engineering, Arizona State University, P.O. Box 875706, Tempe AZ 85284, USA

Abstract

Highly flexible modules using thin 153 cm^2 silicon crystalline cells and transparent fluoropolymer foil are demonstrated. The modules can be flexed 200 times around a bend radius of 4 cm without change in efficiency. The silicon crystalline heterojunction solar cells are 65±5 μm-thick with efficiencies up to 18.4%. Cracks in the solar cells and interconnections that are induced by mechanical stress during module bending are examined using electroluminescence. Two interconnection solutions are discussed: ribbons affixed to the busbars using a conductive adhesive, and indium coated wires directly bonded to the cell fingers. Modules using wire interconnection are found to be highly flexible with efficiencies greatly exceeding existing commercial flexible modules using thin films and have potential applications in light-weight modules for building integrated and portable photovoltaic power.

Peer review by the scientific conference committee of SiliconPV 2016 under responsibility of PSE AG.

Keywords: flexible; module; silicon; heterojunction

1. Introduction

Since 2011 the balance-of-system (BOS) is the leading cost in PV [1,2]. In the period of 2011-2015 $4 billion were invested in PV innovation, and 17%, was on BOS technology. Mounting and racking systems segment account 7-10% of the total cost of the installed photovoltaic system, with estimated market size of $6billion [3].

Lightweight modules have the potential to reduce the BOS cost and increase PV deployment [4]. Lighter and more flexible modules enable PV on weight-constrained roofs (e.g. industrial roofs) and their compact size reduces the transportation costs across supply chain. The installation on roofs is less costly, safer, and minimalist mounting setups are available (e.g. adhesive mounts). They are generally more aesthetically pleasing and the fluoropolymer commonly used as front sheet has typically over 95% optical transparency with lower the glare that allows module use where glare is a critical safety issue (e.g. airports). To succeed the modules must improve not only the power-to-weight ratio, but also the power-to-area performance. Traditionally lightweight and flexible modules are associated

Peer review by the scientific conference committee of SiliconPV 2016 under responsibility of PSE AG.
doi:10.1016/j.egypro.2016.07.132

with organic and thin films deposited over flexible substrates [5,6]. In these devices the power-to-area performance is low. In recent years, new players [7-10] are pursuing a different strategy that uses high efficiency crystalline silicon solar cells instead of using thin film technologies. To reduce weight, a thin transparent polymer replaces the front glass and the structural component is a rigid back sheet that replaces the aluminium frame. The weight savings are up to 85% over a typical glass/tedlar/aluminium frame module. We estimate that our modules will be 10 times lighter per watt-peak than conventional crystalline silicon modules while maintaining similar power-to-area performance. However, the absence of glass and aluminium frame makes the module structurally less rigid and also more vulnerable to mechanical/environmental hazards. The most pressing challenges are [4,11]: cracks in the solar cells and ribbons due to mechanical stress as a result of bending during manufacturing and installation, cracks as result of increased thermally induced stress due to the mismatch of thermal expansion coefficient of the polymer components and the silicon cells, mechanical impact due to hail, corrosion due to increased moisture permeation through the polymeric front/back-sheet and, and encapsulant degradation due to increased moisture ingress and UV radiation. In this manuscript, we address many of these issues by using thin flexible crystalline silicon cells that bend under stress rather than break like conventional cells.

The availability of flexible and high performance solar cells based on a cost competitive and high manufacturing throughput technology provide an opportunity for new range of applications - particularly in building integration PV (BIPV) [12] and portable PV devices. We test the flexibility of the cells and interconnections beyond the requirements for semi-rigid lightweight modules to understand the likely failure mechanism in long term and extreme use.

2. Experiment

2.1. Solar cells

In thin wafers, nearly all minority carriers reach one of the surfaces within their lifetimes and the quality of the surface passivation is critical to mitigate recombination of the carriers [13]. The crystalline silicon heterojunction (SHJ) architecture provides high quality passivation by using hydrogenated intrinsic amorphous silicon (a-Si:H) [14] as buffer layer separating the absorber from highly recombination-active (ohmic) contacts [15]. The cells are prepared on five-inch n-type Czochralski wafers with 3-4 Ω.cm resistivity and initial thickness of 145 µm. The wafers are thinned to 65±5 µm and textured using alkaline wet etching, followed by wet chemical cleaning. The heterojunction is formed using plasma enhanced chemical vapor deposition (PECVD) to grow intrinsic and doped a-Si:H layers (7-10 nm) on both sides of the wafer as shown in Fig. 1 below. Hydrogen plasma treatment improves the performance of the intrinsic layer [16] by restructuring the film during growth. Indium tin oxide (ITO) is sputtered on both sides of the wafer, and silver on the rear as a mirror and rear contact. The front metallization is screen printed silver. The collecting junction can be either in the front or rear side of the cell, greatly simplifying the interconnection of the cells and the encapsulation processes.

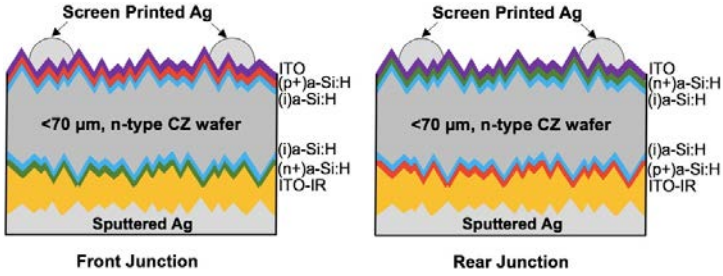

Fig. 1. SHJ cell with front and rear junction. The cells have comparable performances.

2.2. Modules

Two distinctive cell interconnections are examined: traditional ribbons affixed to the busbars using a Z-axis conductive adhesive, and indium coated wires. The wires induce lower mechanical stress on the cells, reduce the shading area, and require less silver paste during the previous printing step [17]. Fig. 2 shows the cell encapsulation with ribbons and wires. The module with wires has an extra polyethylene layer to force the wires against the fingers of the cell. Indium has a melting point of 156 ^{0}C that is close to the lamination temperature of 150 ^{0}C and allows the indium to melt during lamination, creating a good electrical contact. The lamination was performed at 150 ^{0}C for 5 min.

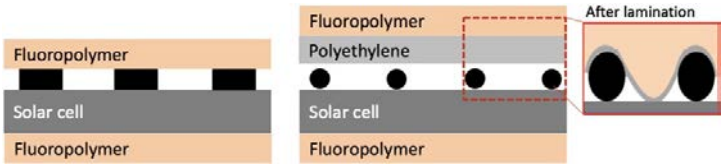

Fig. 2. The black squares (left) represent the ribbons and the black circles (right) the indium-wires. The ribbons were affixed to the busbars using a Z-axis conductive adhesive, and the the wires were fasted against the fingers with the help of the polyethylene layer. In the wires configuration there is no need for busbars, but in this case the busbars were kept to measure the electrical properties before encapsulation. The fluoropolymer is 200 μm-thick and the polyethylene is 80 μm-thick. The ribbons thickness is 130 μm and the wires thickness is 200 μm.

To study the flexibility of the modules, one-cell modules were manufactured with three different interconnections: ribbons 4 mm-wide, ribbons 2 mm-wide, and indium coated wires 0.2 mm-diameter (effective shading 0.15 mm). The ribbons are tin coated and they are 0.13 mm-thick. The total shading area due to wiring is 1.5%, and 3.7% due to busbars. To compare the electrical properties of the cell and module all cells are printed with busbars. In the final design of wire interconnected modules the busbars on the cells (and their attendant shading loss) would be eliminated. The modules are stress tested using the same procedure for testing thin film modules by flexing around cylinders with three radiuses: 8 cm, 6 cm, and 4 cm. The modules are flexed 100 times for each cylinder. The 6 cm and 4 cm tests are very extreme for applications like lightweight modules, but are useful to understand the limits of the modules, and the range of applications. Electroluminescence (EL) imagining is used to inspect the cell cracking, and the electrical performance is measured after each bending step with a IV flash tester.

Alternating front-junction and rear-junction SHJ cells enables direct series interconnection of equivalent sides, i.e. front-to-front and back-to-back of neighbouring cells, as shown in Fig.3. With this arrangement the module manufacturing process is more streamlined and the resulting package is fully planar. The cells can also be assembled closer together and the yield of the module packaging process is improved. The challenge with this solution is to have cells with similar electrical properties, especially in terms of current [18]. The front and rear junction cells in this study have electrical properties are very similar [19] as the cells are well passivated by the amorphous silicon and the diffusion length of the minority carriers is high in the n-type base. As in the case of the single cell module, the performance of the interconnected cells is examined using electroluminescence.

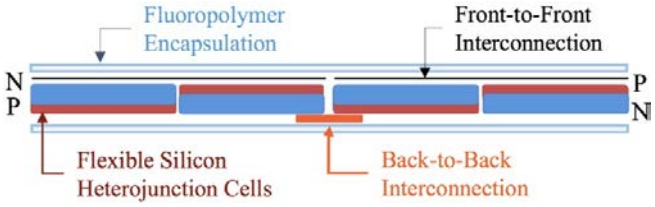

Fig. 3. Front-to-front and back-to-back direct connection of thin cells with front and rear junction.

3. Results and discussion

Thin cells (60 µm-thick) have lower generation current (as measured by integration of the QE) than equivalent thicker cells (125 µm-thick) due to poor absorption of silicon in the infrared. The losses in measured generation current are 1.2±0.25 mA cm^{-2}. The external quantum efficiency (EQE) shows that the cells response starts to diverge for wavelengths over 950 nm, Fig. 4(a). In silicon, the absorption depth [20] for wavelengths greater than 950 nm is over 60 µm, and for 1000 nm is over 150 µm, Fig. 4(b).

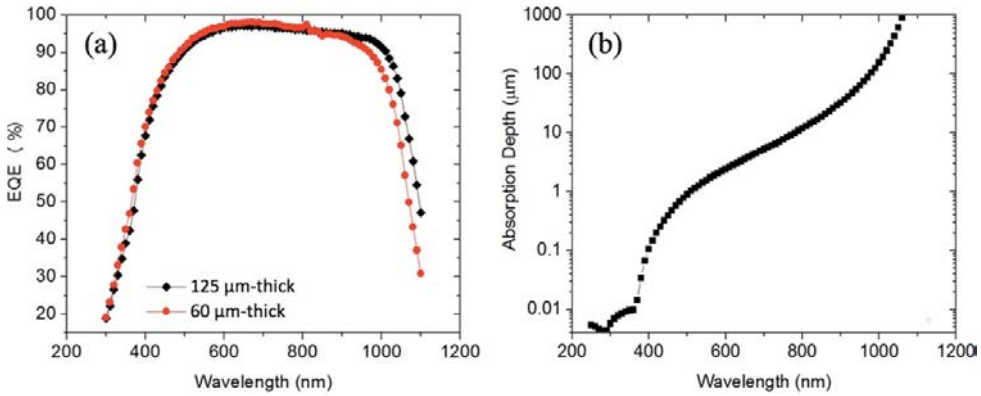

Fig. 4. (a) EQE of 125 µm and 60 µm-thick cell, with generation currents of 39.7 mA cm^{-2} and 38.7 mA cm^{-2}, respectively. (b) Absorption depth in silicon.

The fluoropolymer encapsulation introduces losses in the generation current of 1.6±0.2 mA cm^{-2} with most of the losses are in the UV region as shown in Fig. 5. The UV absorption is well known for glass and ethylene vinyl acetate (EVA) encapsulation. There is also an additional loss due to the anti-reflection coating of the cell not being optimized for encapsulation.

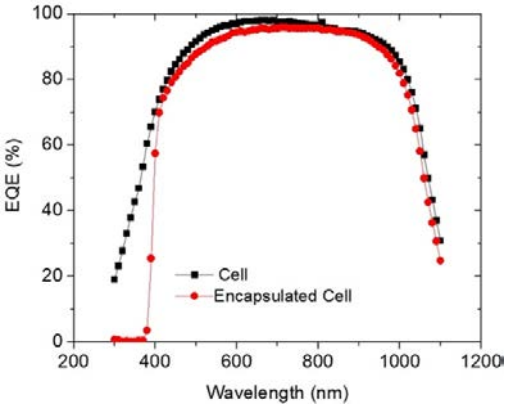

Fig. 5. EQE of 60 µm-thick cell before and after the encapsulation with fluoropolymer. The generations currents are 38.7 mA cm^{-2} and 36.9 mA cm^{-2}, respectively.

The long wavelength losses due to the cell thickness are directly seen in measured short-circuit current losses. However, the flash light has poor emission for wavelengths below 400 nm so the detrimental effect of the fluoropolymer is not so apparent in the short-circuit current measurement. The short-circuit decrease after

encapsulation is 0.6±0.2 mA cm^{-2}. If the extra shading caused by the interconnections is corrected, the current losses are decreased to 0.2±0.2 mA cm^{-2}. Since the short-circuit currents are very close before and after encapsulation the efficiencies of the cell and the respective one-cell module are close. Before encapsulation, the best cell efficiency is 18.4%, open-circuit voltage 737 mV, short-circuit current 34.5 mA cm^{-2} and fill-factor 72.3%. After encapsulation the one-cell module efficiency is 18.4%, open-circuit voltage 737 mV, short-circuit current 34.5 mA cm^{-2} (area correction applied) and fill-factor 72.2%. In Fig. 6. is shown the electrical properties of the cells and modules for this experiment.

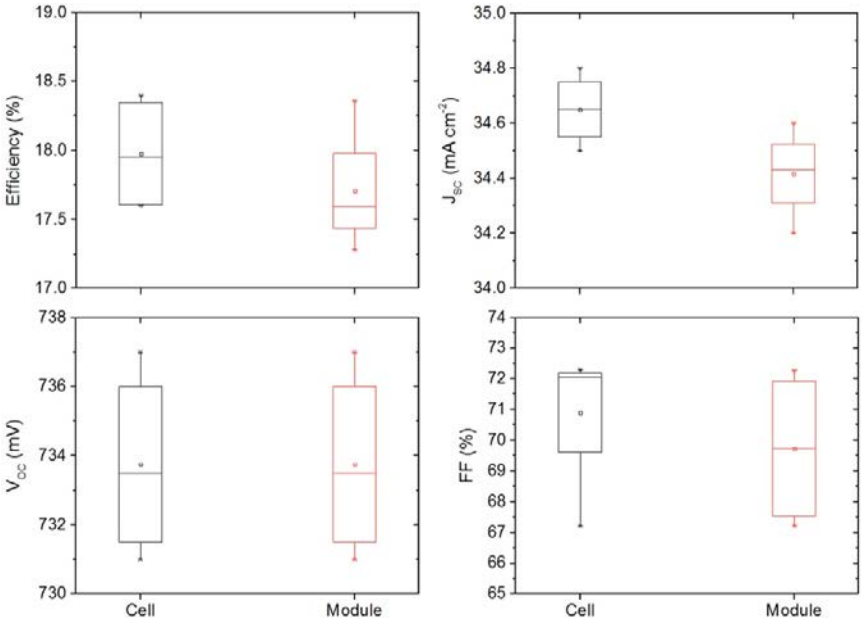

Fig. 6. Electrical properties of 30 cells and the respective one-cell module. 15% of the cells were encapsulated using wires, and the rest of the cells were evenly distributed between 4 mm and 2 mm wide ribbons. The area of the modules was adjusted to correct for the extra shading caused by the ribbons and wires. Process variation causes the variability in plots and there was no significant difference between front and rear junction cells or the efficiency of the modules using ribbons and wires.

One of the main goals of this experiment was to understand how the interconnections affect the flexibility of the module using the procedure outlined in the previous section. The module using the wider ribbons (4 mm wide) cracked after flexing around the 6 cm radius cylinder. When the width of the ribbon was reduced to 2 mm, the module was flexed for 100 times around the 6 cm radius cylinder without any loss in performance. However, the same module cracked after flexing around the 4 cm radius cylinder. The EL images in Fig. 7, demonstrate that the cracks initiate next to the ribbons. When the ribbons are replaced by 0.2 mm-diameter indium coated wires, the module can be flexed 200 times to bend radius of 4 cm without change in efficiency.

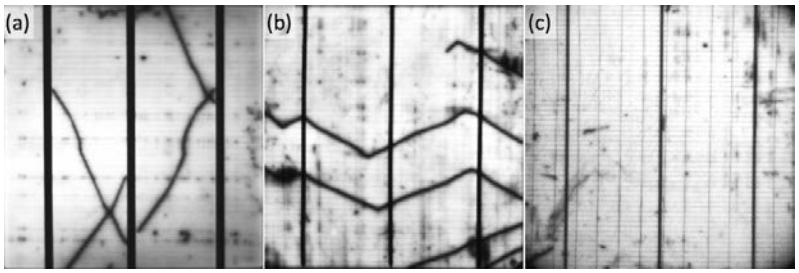

Fig. 7. EL images of one-cell modules: (a) Ribbon 4 mm-wide, the module cracked after flexed to 6 cm bend radius. (b) Ribbon 2 mm-wide, the module cracked after flexed to 4 cm bend radius. (c) Indium coated wires, the module didn't crack after flexed to 4 cm bending radius. The tested cells were 100 cm^2 and 153 cm^2.

Fig. 8 shows the EL image of the first 60 μm-thick two-cell module produced in our lab using indium coated wires and the planar connection scheme utilizing front and rear junction cells. The EL images shows that the wires have correctly bonded to the underlying screen printed fingers as evidenced by the lack of bright regions adjacent to the wires. Across the cells there are multiple dark regions of lower performance. These dark regions are also present before the cells is encapsulated and largely come from silicon surface defects before passivation with a-Si. For instance, the cell on the left shows a vertical line pattern in the EL image unconnected with the wires and the cell on the right shows a horizontal pattern of lines. In both cases the line pattern originates from wafer sawing and it is remarkable that etch process preserves the pattern despite the considerable thinning of the wafers. While the dark regions are quite prominent in the EL images they do not have a large effect on cell performance as evidenced by the high V_{OC} of these cells.

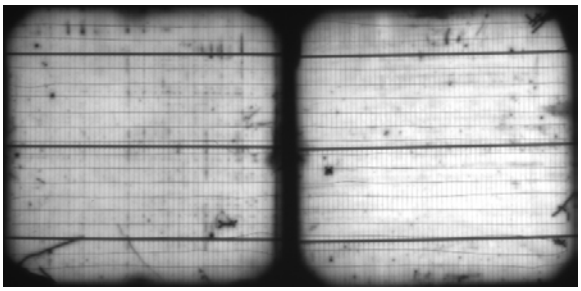

Fig. 8. EL image of two-cells module using 153 cm^2 and 60 μm-thick cells. The busbars are not taking any role in the measurement.

4. Conclusions

Flexible one-cell modules show efficiencies very close to the original cell. The best flexible module uses cells 60 μm-thick with an efficiency of 18.4%. The flexibility of the module is constrained by the type of interconnection and not by the solar cell flexibility. Cracks are initiated next to the ribbons that are affixed to the busbars. Using 0.2 mm-diameter indium coated wires, modules can be flexed 200 times to bend radius of 4 cm without change in efficiency or damage to the cells. The electroluminescence images of the 60 μm-thick two-cell module is a good indication about the quality of the direct front-to-front series connection between front and rear junction cells.

Acknowledgements

This material is based upon work supported in part by the National Science Foundation (NSF) and the Department of Energy (DOE) under cooperative agreement No. EEC-1041895. This work is also supported by the Department of Defense (DOD) Proposal #: DODRIF13-OEPP01-P-0020, and contributions from PowerFilm, Inc.

References

[1] Photovoltaic (PV) Pricing Trends: Historical, Recent, and Near Term Projections, SunShot, US Department of Energy 2012
[2] http://www.greentechmedia.com/articles/read/Solar-Balance-of-System-Accounts-for-68-of-PV-System-Pricing-New-GTM-Repo
[3] Q. Rivoyre, White Paper: PV-Balance of systems innovation reducing installed costs, i3 – Cleantech Group, June 2015
[4] C. Schmid, http://www.pv-tech.org/guest-blog/lightweight_module_durability_working_to_address_a_market_barrier, 02-03-2015
[5] Y. Vygranenko, A. Khosropour, R. Yang, A. Sazonov, A. Kosarev, A. Abramov, and E. Terukov, Canadian Journal of Physics 92, 871 (2014)
[6] P. Reinhard, A. Chirilă, P. Blösch, F. Pianezzi, S. Nishiwaki, S. Buecheler, and A. N. Tiwari, IEEE Journal of Photovoltaics, 3, 572 (2013)
[7] Lumeta Solar, http://www.lumetasolar.com
[8] Giga Solar, http://www.gigasolarpv.com
[9] SMB Solar, http://sbmsolar.com/home/sbm_solar-home.php
[10] Solbian Solar, http://www.solbian.eu/index.php?lang=en
[11] Musa T. Zarmai, N.N. Ekere, C.F. Oduoza, and Emeka H. Amalu, Applied Energy 154, 173 (2015)
[12] T. Schuetze, Energies 6, 2982 (2013)
[13] B. Terheiden, et al., Phys. Status Solidi A, 1 (2014)
[14] J. I. Pankove and M. L. Tarng, Appl. Phys. Lett. 34, 156 (1979)
[15] S. Wolf, A. Descoeudres, Z. C. Holman, and C. Ballif, Green, Vol. 2, 7 (2012)
[16] M. Mews, Mathias Mews, T. Schulze, N. Mingirulli, and Lars Korte1, Appl. Phys Lett. 102, 122106 (2013)
[17] P. Papet, L. Andreetta , D. Lachenal, G. Wahli, J. Meixenberger, B. Legradic, W. Frammelsberger, D. Bätznera, B. Straha, Y. Yao, and T. Söderström, Energy Procedia 67, 203 (2015)
[18] T. Buck, R. Kopecek, J. Libal, R. Petres, K. Peter, I. Rover, K. Wambach, L. J. Geerligs, E. Wefringhaus, and P. Fath, in Proceedings of IEEE 4th World Conference. Waikoloa, 1060 (2006)
[19] S. Y Herasimenka, W. J Dauksher, C. J Tracy, J. Lee, A. Augusto, H. Jain, K. Tyler, Z. Kiefer, P. Balaji, S. G. Bowden and C. Honsberg, in Proceedings of 31st European Photovoltaic Solar Energy Conference and Exhibition, 761 (2015)
[20] M.A. Green, and M. Keevers, Progress in Photovoltaics 3, 189 (1995)